Proceedings of the ASME 2017 International Design Engineering Technical Conferences &
Computers and Information in Engineering Conference
IDETC/CIE 2017
August 6-9, 2017, Cleveland, Ohio, USA

SAND2017-4940C

DETC2017-67553

ON HURTY/CRAIG-BAMPTON SUBSTRUCTURING WITH INTERFACE REDUCTION ON CONTACTING SURFACES

Robert J. Kuether
Sandia National Laboratories
Albuquerque, New Mexico, USA

Peter B. Coffin
Sandia National Laboratories
Albuquerque, New Mexico, USA

Adam R. Brink
Sandia National Laboratories
Albuquerque, New Mexico, USA

ABSTRACT

Structural dynamics models with localized nonlinearities can be reduced using Hurty/Craig-Bampton component mode synthesis methods. The interior degrees-of-freedom of the linear subcomponents are reduced with a set of dynamic fixed-interface modes while the static constraint modes preserve the physical coordinates at which the nonlinear restoring forces are applied. For finite element models with a highly refined mesh at the boundary, a secondary modal analysis can be performed to reduce the interface down to a truncated set of local-level characteristic constraint modes. In this research, the cost savings and accuracy of the interface reduction technique are evaluated on a simple example problem involving two elastic blocks coming into contact.

INTRODUCTION

Nonlinear structural dynamic models often consist of a set of linear substructures connected through a nonlinear constitutive law that acts locally on the interface(s). Typical localized nonlinearities include friction or contact, and connections with bilateral or nonlinear stiffness characteristics. Since the interior portion of the linear models do not have nonlinear restoring forces, component mode synthesis methods are well suited to reduce the interior portion with a set of dynamic modes while retaining the boundary degrees-of-freedom (DOF) for the nonlinear forces to act.

Substructuring methods can be categorized as free- or fixed-interface methods, or hybrid methods. Two of the commonly referenced free-interface approaches include the Rubin method [1] and the MacNeal method [2]. The most well-known fixed-interface approach is the Hurty/Craig-Bampton (HCB) method that was originally proposed by Hurty in 1960 [3] and later simplified by Craig and Bampton in [4]. The HCB method reduces each subcomponent using a truncated set of fixed-interface (FI) vibration modes along with a set of static constraint modes. Finite element models tend to have highly refined meshes at the interface resulting in a reduced order model with a prohibitively large number of DOF retained at the boundary. Many types of interface reduction techniques have been developed to further decrease the model size; a review of these methods for HCB models can be found in [5].

In this research, the HCB method with local-level interface reduction [6] is used to model two substructures coming into contact with one another in an effort to reduce the computational cost associated with numerical time integration. The contact at the interface is modeled using the penalty method and there are no friction forces enabled during the simulation. This research explores HCB models of varying basis fidelity as a starting point to understand whether a significant number of modes can be truncated and still capture the rebound characteristics of two elastic substructures.

THEORY

Hurty/Craig-Bampton Substructures

The finite element models of interest are linear subcomponents that interact with one another at the boundary DOF via frictionless contact. It is assumed that each substructure individually behaves linearly and that the introduction of contact forces at the interface is the only source of nonlinearity. While many reduction schemes are available for representing linear subcomponent models, this work starts with the HCB equations of motion [4, 7] to reduce each linear subcomponent with the mathematical form,

$$\begin{bmatrix} \mathbf{I}_{kk} & \hat{\mathbf{M}}_{kb} \\ \hat{\mathbf{M}}_{bk} & \hat{\mathbf{M}}_{bb} \end{bmatrix} \begin{Bmatrix} \ddot{\mathbf{q}}_k \\ \ddot{\mathbf{x}}_b \end{Bmatrix} + \begin{bmatrix} \mathbf{\Lambda}_{kk} & \mathbf{0}_{kb} \\ \mathbf{0}_{bk} & \hat{\mathbf{K}}_{bb} \end{bmatrix} \begin{Bmatrix} \mathbf{q}_k \\ \mathbf{x}_b \end{Bmatrix} = \begin{Bmatrix} \mathbf{0} \\ \mathbf{f}(t) + \mathbf{r}(t) \end{Bmatrix} \quad (1)$$

The $N_k \times 1$ vector $\mathbf{q}_k$ represents the fixed-interface modal coordinates and the $N_b \times 1$ vector $\mathbf{x}_b$ corresponds to the physical boundary DOF. The overdot represents the derivative with respect to time and the $N_b \times 1$ vector $\mathbf{f}(t)$ corresponds to externally applied forces. The unknown $N_b \times 1$ vector $\mathbf{r}(t)$ is included to account for the unknown forces applied at the boundary through interactions with adjacent structures.

Without loss of generality, assume that two subcomponents are defined with superscripts (A) and (B). During the assembly process, the contact model is applied only at the physical boundary DOF, $\mathbf{x}_b$. These interface forces replace the unknown reaction force, $\mathbf{r}(t)$, resulting in the assembled equations of motion,

$$\begin{bmatrix} \mathbf{I}_{kk}^{(\mathrm{A})} & \hat{\mathbf{M}}_{kb}^{(\mathrm{A})} & \mathbf{0} & \mathbf{0} \\ \hat{\mathbf{M}}_{bk}^{(\mathrm{A})} & \hat{\mathbf{M}}_{bb}^{(\mathrm{A})} & \mathbf{0} & \mathbf{0} \\ \mathbf{0} & \mathbf{0} & \mathbf{I}_{kk}^{(\mathrm{B})} & \hat{\mathbf{M}}_{kb}^{(\mathrm{B})} \\ \mathbf{0} & \mathbf{0} & \hat{\mathbf{M}}_{bk}^{(\mathrm{B})} & \hat{\mathbf{M}}_{bb}^{(\mathrm{B})} \end{bmatrix} \begin{Bmatrix} \ddot{\mathbf{q}}_k^{(\mathrm{A})} \\ \ddot{\mathbf{x}}_b^{(\mathrm{A})} \\ \ddot{\mathbf{q}}_k^{(\mathrm{B})} \\ \ddot{\mathbf{x}}_b^{(\mathrm{B})} \end{Bmatrix} + \ldots$$
$$\begin{bmatrix} \mathbf{\Lambda}_{kk}^{(\mathrm{A})} & \mathbf{0} & \mathbf{0} & \mathbf{0} \\ \mathbf{0} & \hat{\mathbf{K}}_{bb}^{(\mathrm{A})} & \mathbf{0} & \mathbf{0} \\ \mathbf{0} & \mathbf{0} & \mathbf{\Lambda}_{kk}^{(\mathrm{B})} & \mathbf{0} \\ \mathbf{0} & \mathbf{0} & \mathbf{0} & \hat{\mathbf{K}}_{bb}^{(\mathrm{B})} \end{bmatrix} \begin{Bmatrix} \mathbf{q}_k^{(\mathrm{A})} \\ \mathbf{x}_b^{(\mathrm{A})} \\ \mathbf{q}_k^{(\mathrm{B})} \\ \mathbf{x}_b^{(\mathrm{B})} \end{Bmatrix} + \begin{Bmatrix} \mathbf{0} \\ \mathbf{f}_{NL}\left(\mathbf{x}_b^{(\mathrm{A})}, \mathbf{x}_b^{(\mathrm{B})}\right) \\ \mathbf{0} \\ -\mathbf{f}_{NL}\left(\mathbf{x}_b^{(\mathrm{A})}, \mathbf{x}_b^{(\mathrm{B})}\right) \end{Bmatrix} = \begin{Bmatrix} \mathbf{0} \\ \mathbf{f}(t)^{(\mathrm{A})} \\ \mathbf{0} \\ \mathbf{f}(t)^{(\mathrm{B})} \end{Bmatrix} \quad (2)$$

The nonlinear contact forces generally depend on the physical displacements, $\mathbf{x}_b$, as well as the undeformed position of each node. The frictionless contact model is described in more detail later in the theory section.

Interface Reduction

The model in Eq. (2), with an appropriately defined contact algorithm, is integrated numerically in time using central difference explicit time integration. This direct integration scheme is conditionally stable and the time step is dictated by the highest frequency in the system of equations. The critical time step for the central difference scheme [8] is defined as,

$$\Delta t_{cr} = \frac{2}{\omega_{\max}} \quad (3)$$

The frequency $\omega_{\max}$ corresponds to the highest natural frequency of the assembled eigenvalue problem, $\left(\hat{\mathbf{K}} - \omega^2 \hat{\mathbf{M}}\right)\boldsymbol{\varphi} = \mathbf{0}$, from the model in Eq. (2) that accounts for the penalty stiffness at the interface. The highest frequency content generally comes from the retention of the static constraint modes due to their localized kinematics. In an effort to increase the critical time step as well as further reduce the model size, an interface reduction step is applied to the boundary DOF using the local characteristic constraint (L-CC) modes described in [5, 6, 9].

Starting with the HCB subcomponent model in Eq. (1), the L-CC modes are computed from a secondary modal analysis on the boundary partition of the mass and stiffness matrices,

$$\left(\hat{\mathbf{K}}_{bb} - \omega^2 \hat{\mathbf{M}}_{bb}\right)\boldsymbol{\varphi}^{CC} = \mathbf{0} \quad (4)$$

where $\boldsymbol{\varphi}^{CC}$ is the local characteristic constraint mode with corresponding natural frequency, ω. The L-CC modes are truncated and used to assemble the secondary subcomponent transformation matrix,

$$\begin{Bmatrix} \mathbf{q}_k \\ \mathbf{x}_b \end{Bmatrix} = \begin{bmatrix} \mathbf{I} & \mathbf{0} \\ \mathbf{0} & \mathbf{\Phi}^{CC} \end{bmatrix} \begin{Bmatrix} \mathbf{q}_k \\ \mathbf{q}_c \end{Bmatrix} = \mathbf{T}^{CC} \begin{Bmatrix} \mathbf{q}_k \\ \mathbf{q}_c \end{Bmatrix} \quad (5)$$

The $N_c \times 1$ vector $\mathbf{q}_c$ corresponds to the L-CC generalized coordinates. Applying this transformation to Eq. (1) results in,

$$\begin{bmatrix} \mathbf{I}_{kk} & \hat{\mathbf{M}}_{kb}\mathbf{\Phi}^{CC} \\ \mathbf{\Phi}^{CC\mathrm{T}}\hat{\mathbf{M}}_{bk} & \mathbf{\Phi}^{CC\mathrm{T}}\hat{\mathbf{M}}_{bb}\mathbf{\Phi}^{CC} \end{bmatrix} \begin{Bmatrix} \ddot{\mathbf{q}}_k \\ \ddot{\mathbf{q}}_c \end{Bmatrix} + \ldots$$
$$\begin{bmatrix} \mathbf{\Lambda}_{kk} & \mathbf{0}_{kb} \\ \mathbf{0}_{bk} & \mathbf{\Phi}^{CC\mathrm{T}}\hat{\mathbf{K}}_{bb}\mathbf{\Phi}^{CC} \end{bmatrix} \begin{Bmatrix} \mathbf{q}_k \\ \mathbf{q}_c \end{Bmatrix} = \begin{Bmatrix} \mathbf{0} \\ \mathbf{\Phi}^{CC\mathrm{T}}\left(\mathbf{f}(t) + \mathbf{r}(t)\right) \end{Bmatrix} \quad (6)$$

which is more compactly rewritten as,

$$\begin{bmatrix} \mathbf{I}_{kk} & \tilde{\mathbf{M}}_{kc} \\ \tilde{\mathbf{M}}_{ck} & \tilde{\mathbf{M}}_{cc} \end{bmatrix} \begin{Bmatrix} \ddot{\mathbf{q}}_k \\ \ddot{\mathbf{q}}_c \end{Bmatrix} + \begin{bmatrix} \mathbf{\Lambda}_{kk} & \mathbf{0}_{kc} \\ \mathbf{0}_{ck} & \tilde{\mathbf{K}}_{cc} \end{bmatrix} \begin{Bmatrix} \mathbf{q}_k \\ \mathbf{q}_c \end{Bmatrix} = \begin{Bmatrix} \mathbf{0} \\ \tilde{\mathbf{f}}(t) + \tilde{\mathbf{r}}(t) \end{Bmatrix} \quad (7)$$

Assembling the equations of motion for substructure (A) and (B) results in

$$\begin{bmatrix} \mathbf{I}_{kk}^{(\mathrm{A})} & \tilde{\mathbf{M}}_{kc}^{(\mathrm{A})} & \mathbf{0} & \mathbf{0} \\ \tilde{\mathbf{M}}_{ck}^{(\mathrm{A})} & \tilde{\mathbf{M}}_{cc}^{(\mathrm{A})} & \mathbf{0} & \mathbf{0} \\ \mathbf{0} & \mathbf{0} & \mathbf{I}_{kk}^{(\mathrm{B})} & \tilde{\mathbf{M}}_{kc}^{(\mathrm{B})} \\ \mathbf{0} & \mathbf{0} & \tilde{\mathbf{M}}_{ck}^{(\mathrm{B})} & \tilde{\mathbf{M}}_{cc}^{(\mathrm{B})} \end{bmatrix} \begin{Bmatrix} \ddot{\mathbf{q}}_k^{(\mathrm{A})} \\ \ddot{\mathbf{q}}_c^{(\mathrm{A})} \\ \ddot{\mathbf{q}}_k^{(\mathrm{B})} \\ \ddot{\mathbf{q}}_c^{(\mathrm{B})} \end{Bmatrix} + \ldots$$
$$\begin{bmatrix} \mathbf{\Lambda}_{kk}^{(\mathrm{A})} & \mathbf{0} & \mathbf{0} & \mathbf{0} \\ \mathbf{0} & \tilde{\mathbf{K}}_{cc}^{(\mathrm{A})} & \mathbf{0} & \mathbf{0} \\ \mathbf{0} & \mathbf{0} & \mathbf{\Lambda}_{kk}^{(\mathrm{B})} & \mathbf{0} \\ \mathbf{0} & \mathbf{0} & \mathbf{0} & \tilde{\mathbf{K}}_{cc}^{(\mathrm{B})} \end{bmatrix} \begin{Bmatrix} \mathbf{q}_k^{(\mathrm{A})} \\ \mathbf{q}_c^{(\mathrm{A})} \\ \mathbf{q}_k^{(\mathrm{B})} \\ \mathbf{q}_c^{(\mathrm{B})} \end{Bmatrix} + \begin{Bmatrix} \mathbf{0} \\ \mathbf{\Phi}^{CC,(A)\mathrm{T}}\mathbf{f}_{NL}\left(\mathbf{q}_c^{(\mathrm{A})}, \mathbf{q}_c^{(\mathrm{B})}\right) \\ \mathbf{0} \\ -\mathbf{\Phi}^{CC,(B)\mathrm{T}}\mathbf{f}_{NL}\left(\mathbf{q}_c^{(\mathrm{A})}, \mathbf{q}_c^{(\mathrm{B})}\right) \end{Bmatrix} = \begin{Bmatrix} \mathbf{0} \\ \tilde{\mathbf{f}}(t)^{(\mathrm{A})} \\ \mathbf{0} \\ \tilde{\mathbf{f}}(t)^{(\mathrm{B})} \end{Bmatrix} \quad (8)$$

Now the contact forces are explicitly computed through the L-CC generalized coordinates, $\mathbf{q}_c$, using the transformation between physical and modal DOF.

Contact Modeling

A penalty method [10] is used to enforce the contact constraint at the boundary DOF of the HCB model. The constraint between two contacting node pairs is defined such that the gap must either be open or closed with no overlap. Mathematically, this is written as,

$$g(\mathbf{x}_b) \geq 0 \tag{9}$$

The gap, $g(\mathbf{x}_b)$, is positive when open, negative when the contacting nodes overlap and zero when the nodes are in perfect contact.

The penalty method formulation defines the contact force at a particular node with superscript *j* as,

$$\mathbf{f}_{NL}^{j}(\mathbf{x}_b) = \varepsilon_c \hat{g}^{j}(\mathbf{x}_b)\mathbf{n}^{j} \tag{10}$$

where ε_c is the penalty stiffness value and $\mathbf{n}^j$ is the interface normal direction. The gap used within the contact force equation, $\hat{g}^j(\mathbf{x}_b)$, is defined as,

$$\hat{g}^{j}(\mathbf{x}_b) = \begin{cases} g^{j}(\mathbf{x}_b), & g^{j}(\mathbf{x}_b) < 0 \\ 0, & g^{j}(\mathbf{x}_b) \geq 0 \end{cases} \tag{11}$$

The variable $g^j(\mathbf{x}_b)$ is the gap between node *j* and the opposing contact node. In this research, the contact surface is defined over a mesh where the interface nodes align and the deformations are assumed to be small. This simplifies the analysis by predefining the contact node pairs and assuming these do not change during the simulation.

The gap is computed between two node pairs: *j* on the master node and *m* on the slave node. Thus, the gap becomes,

$$g^{j}(\mathbf{x}_b) = -\left|\mathbf{d}^{jm}\right| \cdot sign\left(\mathbf{d}^{jm} \cdot \mathbf{n}^{j}\right) \tag{12}$$

and the distance vector between the two nodes is,

$$\mathbf{d}^{jm} = \left(\mathbf{X}^{j} + \mathbf{x}^{j}\right) - \left(\mathbf{X}^{m} + \mathbf{x}^{m}\right) \tag{13}$$

The distance is a function of the undeformed nodal position, $\mathbf{X}^j$, and the physical displacement $\mathbf{x}^j$.

NUMERICAL RESULTS

Model Description

The model under consideration consists of two blocks of equal dimensions (25.4 x 38.1 x 50.8 *mm*), separated by an initial 15.24 *mm* gap. Each block is discretized with 400 linear hexahedral elements, resulting in 1,782 DOF, as shown in Fig. 1. The blocks are made of an idealized elastic material with Young's Modulus of 5,171 *GPa*, Poisson's ratio of 0.2 and a mass density of 0.6522 *g/cc*. At the beginning of the analysis, the "right" block has zero initial velocity and the "left" block has an initial velocity of 3,810 *m/s* towards the opposing block. This high initial velocity is selected to reduce overall analysis time. All the nodes on the contacting faces of each block are defined as the boundary DOF for the HCB formulation. This results in two HCB models each having a total of 162 boundary DOF, leaving a possible 1,620 fixed-interface modal DOF.

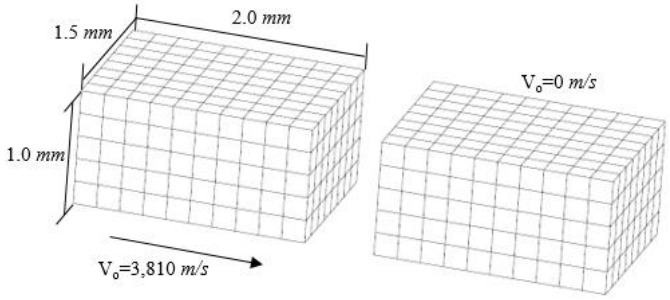

Figure 1. Finite Element Model Under Consideration

The response of the block models is numerically computed with a conditionally stable and second order accurate central difference explicit time integration scheme [8]. A penalty stiffness value of 175E+09 N/m was used to define the node-to-node contact. Preliminary simulations of the impact reveal some common issues related to contact modeling with the penalty method. Defining a penalty stiffness that is too small allows excessive penetration between structures during contact, but too high of stiffness values introduce convergence issues and numerical instabilities. The advantage to using this approach is that it is simple to implement numerically and requires no iterative solvers when using explicit integration schemes.

HCB Model Reduction

The critical time steps were computed for the assembled HCB models with the penalty springs engaged at all the interface DOF; these values are listed in Table 1 for models of varying fixed-interface mode fidelity. The mean solve time corresponds to the amount of CPU time required to solve for 1,000 time steps when the blocks come in and out of contact. The HCB model with 1,619 fixed-interface modes truncates only one fixed-interface mode, so it is assumed to be the reference model for comparison.

Table 1. Comparison of critical time step and solver time for various HCB models

FI Modes per Substructure	Max FI Frequency (Hz)	Δt_{cr} (sec)	Mean Solve Time (sec)	Model Size (DOF)
1619	4.18E+06	1.38E-08	22.6	3562
500	1.76E+06	1.48E-08	2.59	1324
250	1.30E+06	1.49E-08	0.96	824
100	8.49E+05	1.49E-08	0.71	524
20	3.97E+05	1.49E-08	0.67	364
1	3.59E+04	1.49E-08	0.61	326

Truncating the fixed-interface modes drastically reduced the size of the system matrix and the mean solve time, but did not improve the critical time step. When going from 1,619 fixed-interface modes down to one, the critical time step only increased by ~8% but the solve time decreased by 97%! When modeling contact with the penalty method, the critical time step remained unaffected by the truncation of the dynamic modes, but the overall reduction in model size significantly sped up simulation time.

Each of the models presented in Table 1 were used to compare their accuracy relative to the reference solution (i.e. the 1,619 FI mode model) when there is no lateral offset of the impacting interfaces. The time histories of each simulation are shown in Fig. 2; the responses along the vertical axis correspond to the average x-position of all the nodes on the contacting faces. The solid lines correspond to the "left" block assigned with the initial velocity, and the dashed lines are the "right" block which was initially at rest. The blocks first come into contact around 0.4E-05 seconds. After this point, the blocks move in unison until about 0.8E-05 seconds, after which they separate and move forward with different velocities.

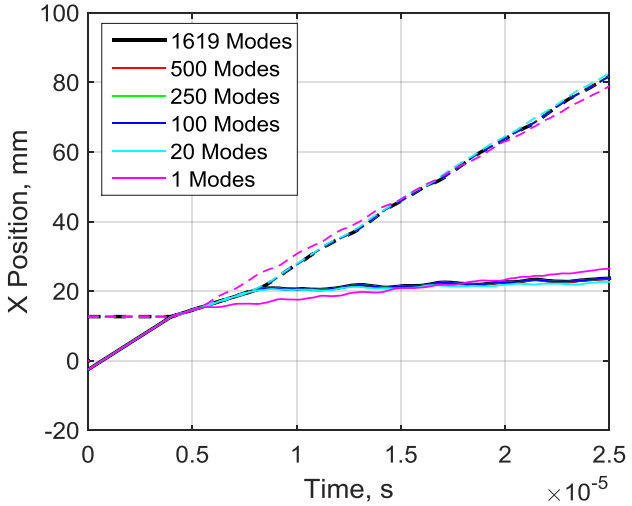

Figure 2. Average Nodal Displacements for Various HCB Models

A comparison of the reduced order models revealed that most of the predicted responses agreed well with the reference solution except for the 1 FI mode model and possibly the 20 FI mode model. Each of the two lowest fidelity models showed some discrepancy when visually comparing the signals. The contact impulse that occurred during impact produced an internal force with a $2/\tau$ frequency of approximately 5.0E+05 Hz. The maximum fixed-interface mode frequencies in Table 1 revealed that the 20 FI mode model only kept modes up to 3.97E+05 Hz and that some of the dynamically important modes were not included in the model. This internal contact force was not known a priori, so it was difficult to know exactly at what frequency to truncate the dynamic modes. However, as with all finite element analyses, a convergence study should be performed to determine when a sufficient number of modes have been included in the basis.

HCB with Interface Reduction

Next, the interface reduction was applied to the boundary DOF of the two HCB models by computing the L-CC modes of the interface partition of each block. Based on the observed accuracy in the previous subsection, an incremental reduction to the interface was applied to the 100 FI mode HCB model. The results in Table 2 compare the maximum characteristic constraint mode frequency, critical time steps, mean solve times, and system model size, exactly as was done in Table 1. The 162 CC mode model was essentially the same as the 100 FI mode HCB model except that the boundary DOF span modal space rather than physical space. Note that the mean solve times increased for the models with the modal interface DOF (i.e. 0.71 sec to 3.33 sec). This cost was associated with the numerical implementation of the penalty method and the added computation needed to transform between modal and physical space at each time step.

Table 2. Comparison of critical time step and solver time for various L-CC interface reduced models

CC Modes per Substructure	Max CC Frequency (Hz)	Δt_{cr} (sec)	Mean Solve Time (sec)	Model Size (DOF)
162	3.56E+06	1.49E-08	3.33	524
100	2.21E+06	2.27E-08	3.42	400
75	1.89E+06	2.65E-08	3.24	350
50	1.46E+06	3.41E-08	3.11	300
25	8.91E+05	4.69E-08	3.01	250
6	0.05E+00	6.42E-08	2.89	212

As the interface was incrementally reduced, two observations were made. First, going from 162 DOF down to 6 DOF increased the critical time step by a factor of about four. Theoretically, this would allow for fewer steps to reach a

predetermined simulation period, hence reducing the cost of numerical time integration. (Care should be taken when increasing the time step with the penalty method, however, since this may produce convergence issues.) The second observation was that there was no drastic improvement in the mean solve time. This could be attributed to the numerical implementation of the penalty method and transformation between physical and modal coordinates, but this issue has not yet been resolved.

The interface reduced models in Table 2 were used to simulate the contact response when there was no lateral offset of the impacting surfaces and the time history results are shown in Fig. 3. As before, the solid line is the "left" block and dashed is the "right", and the plot corresponds to the average x-position of all nodes on the contacting surface.

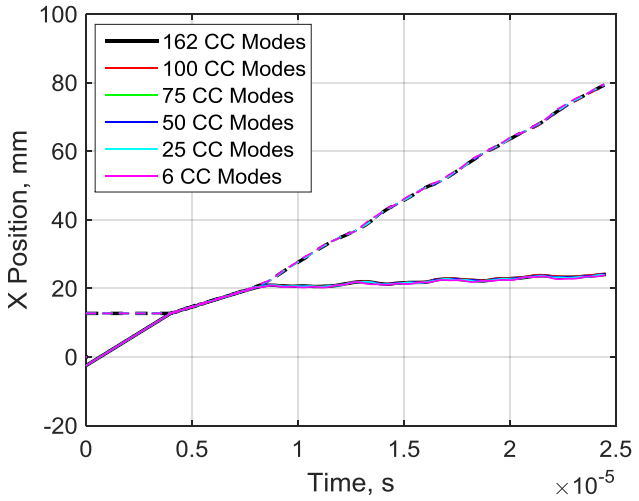

Figure 3. Average Nodal Displacements for Various HCB Models with L-CC Interface Reduction

Visual comparison of the various interface reduced models revealed that all models agreed well with the original HCB model. The 6 CC mode model only included rigid body modes, suggesting that these were the most important to capture the interaction between the two blocks. The fact that the two blocks come into contact in a uniform way suggested that this was a physically reasonable result and that no higher order deformation shapes at the interface were needed to capture the rebound. By going from the 1,619 FI mode HCB model down to the 6 CC mode model, the system model size reduced from 3,562 DOF down to 212 DOF, and the mean solve time for 1,000 time steps went from 22.6 sec down to 2.89 sec. The critical time step went from 1.38E-08 sec to 6.42E-08 sec, all while preserving the accuracy of the reference model.

Blocks with 50% Lateral Offset

The cases studied in the previous two subsections explored in detail the case when the blocks come together in a completely uniform way, such that the interface surfaces had no lateral offset with one another when they came into contact. In this subsection and the next, two other cases are explored such that there was only 50% and 75% lateral offset of the interface surfaces. This was achieved by offsetting the undeformed position of the "left" block by the appropriate amount. The HCB reduced models in Table 1 and the interface reduced models in Table 2 were used to simulate the contact response when the interfaces are offset laterally by 50% and the time history results are shown in Figs. 4 and 5, respectively. These results produced the same conclusions as the no lateral offset case presented earlier. The HCB model required only 100 FI modes due to the period of the contact impulse, and only 6 CC modes (i.e. rigid body modes) were needed to capture the contact interaction with interface reduction.

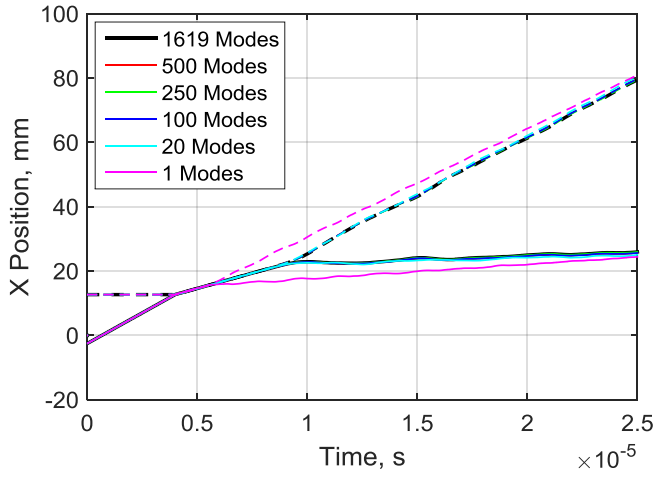

Figure 4. Average Nodal Displacements for Various HCB Models and 50% Lateral Offset

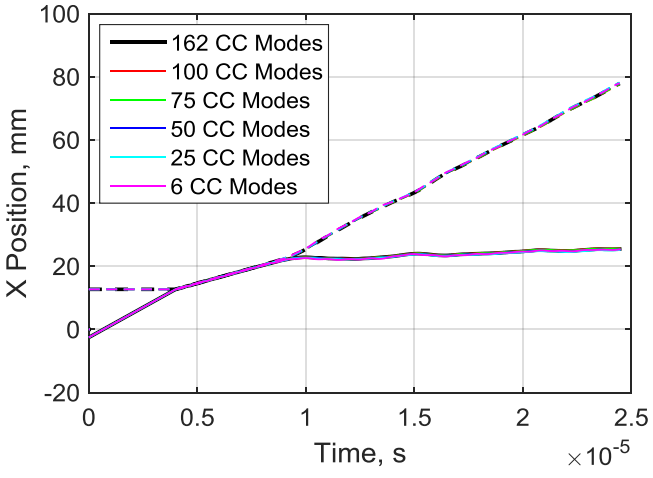

Figure 5. Average Nodal Displacements for Various HCB Models with L-CC Interface Reduction and 50% Lateral Offset

Blocks with 75% Lateral Offset

Here the HCB reduced models in Table 1 and the interface reduced models in Table 2 were used to simulate the contact response when the interfaces had lateral offset of 75%; the time history results are shown in Figs. 6 and 7, respectively. This case produced different conclusions compared to the 50% and 0% lateral offset cases. In the time histories, it was observed that the period of the contact impulse was longer for the 75% lateral offset case. As a result, the $2/\tau$ frequency of the impact force was approximately 3.3E+05 Hz. The 20 FI HCB model performed quite well since the highest FI mode frequency was 4.0E+05 Hz. As discussed earlier, the duration of the contact forces appeared to dictate the number of FI modes needed to retain in basis. Visual inspection of the results from the interface reduced models in Fig. 7 suggested that more than just the 6 CC modes were needed to capture the response of the 75% lateral offset case. The next highest fidelity model with 25 CC modes was deemed accurate enough and appeared to converge with the higher fidelity models. The contact forces occurred over a smaller patch on the interface surface and excited the higher order CC modes during the impact event.

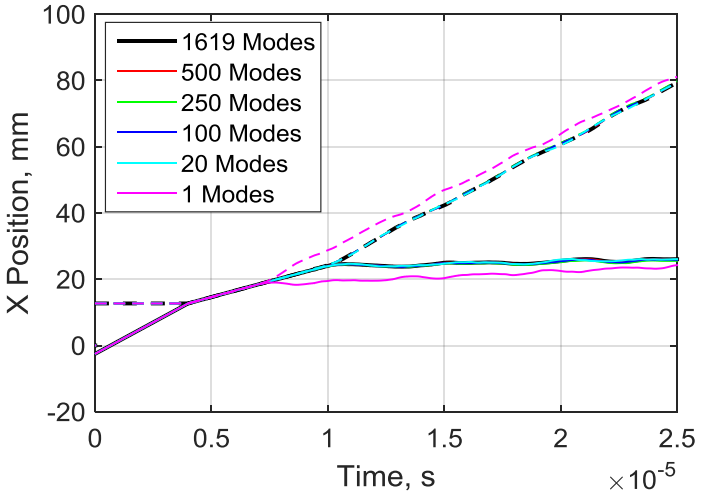

Figure 6. Average Nodal Displacements for Various HCB Models and 75% Lateral Offset

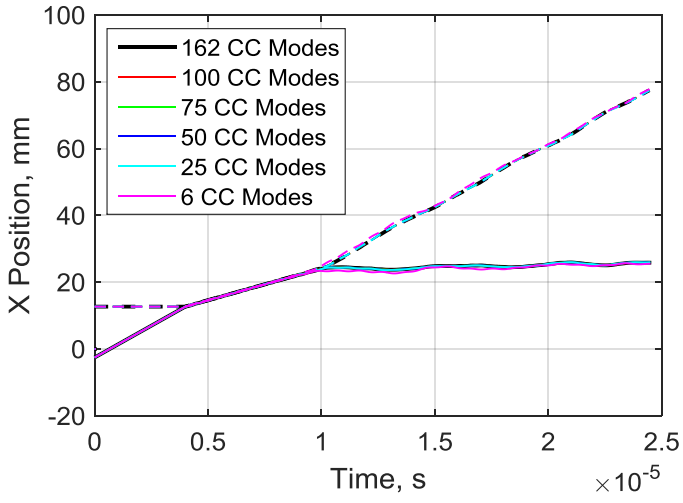

Figure 7. Average Nodal Displacements for Various HCB Models with L-CC Interface Reduction and 75% Lateral Offset

It should be noted here that all of the numerical simulations used the same time step in an effort to make fair comparisons between model fidelities. In practice, it is common to set the time step to 90% of the critical value, but this may be adjusted as necessary to obtain convergence. It was discovered that, for the 25 L-CC mode model, that the 90% critical time step was not sufficient to reach convergence, and that 80% was deemed accurate relative to the reference solution. Analysts should be careful when determining the step size for highly nonlinear problems involving contact.

CONCLUSIONS

The Hurty/Craig-Bampton substructuring method is applied to a finite element model with a frictionless contacting surface and an interface reduction technique is implemented to further reduce the model size and simulation time. The local-level characteristic constraint modes provide a secondary reduction to the HCB method by transforming the physical DOF to a truncated set of interface modes. The contact at the interface is modeled with the penalty method assuming that the deformations are small and that the finite element mesh aligns such that the contacting node pairs are defined a priori. The method is demonstrated on a model where two elastic blocks come into contact and rebound off one another. Three cases are explored such that the interface surfaces have no lateral offset, and are offset by 50% or 75%. The HCB method shows a reduction in the simulation time but no useful increase in the critical time step for the explicit integrator. Comparisons of the time histories suggest that the reduction basis needs fixed-interface modes that capture the $2/\tau$ frequency of the impact force, which depends on the amount of lateral offset on the interface surfaces. As with most finite element analyses, a convergence study should be performed to determine when a

sufficient number of modes has been included in the basis. When applying interface reduction with characteristic constraint modes to the 100 fixed-interface mode HCB model, the model size decreases further and the critical time step increases. The results presented in this research reveal that the required number of characteristic constraint modes depends on the shape of the contact force profile at the interface. In the worst case of 75% lateral offset, the interface reduction increases the critical time step by a factor of about three. This provides a significant improvement in the computational cost associated with numerical time simulations.

This work is a preliminary study to explore the feasibility of using substructuring techniques to reduce the computational burden of models involving contact. Future work will explore other contact models, such as augmented Lagrange multipliers, and the addition of friction laws at the interface.

ACKNOWLEDGMENTS

This work was funded by Sandia National Laboratories. Sandia National Laboratories is a multimission laboratory managed and operated by National Technology and Engineering Solutions of Sandia, LLC., a wholly owned subsidiary of Honeywell International, Inc., for the U.S. Department of Energy's National Nuclear Security Administration under contract DE-NA-0003525.

REFERENCES

[1] S. Rubin, "Improved Component-Mode Representation for Structural Dynamic Analysis," *AIAA Journal*, vol. 13, pp. 995-1006, 1975/08/01 1975.

[2] R. H. MacNeal, "A hybrid method of component mode synthesis," *Computers & Structures*, vol. 1, pp. 581-601, 1971.

[3] W. C. Hurty, "Vibrations of structural systems by component mode synthesis," *Journal of the Engineering Mechanics Division*, vol. 86, pp. 51-70, 1960.

[4] R. R. J. Craig and M. C. C. Bampton, "Coupling of Substructures for Dynamic Analysis," *AIAA Journal*, vol. 6, pp. 1313-1319, 1968.

[5] D. Krattiger, L. Wu, M. Zacharczuk, M. Buck, R. J. Kuether, M. S. Allen, *et al.*, "Interface Reduction for Hurty/Craig-Bampton Substructured Models: Review and Improvements," *Mechanical Systems and Signal Processing (in review)*, 2017.

[6] S.-K. Hong, B. I. Epureanu, and M. P. Castanier, "Next-generation parametric reduced-order models," *Mechanical Systems and Signal Processing*, vol. 37, pp. 403-421, 2013.

[7] R. R. Craig, "Coupling of substructures for dynamic analyses: an overview," in *Proceedings of AIAA/ASME/ASCE/AHS/ASC structures, structural dynamics, and materials conference and exhibit*, 2000, pp. 1573-1584.

[8] R. D. Cook, D. S. Malkus, M. E. Plesha, and R. J. Witt, *Concepts and Applications of Finite Element Analysis*, Fourth ed.: John Wiley and Sons, 2002.

[9] R. J. Kuether, M. S. Allen, and J. J. Hollkamp, "Modal Substructuring of Geometrically Nonlinear Finite Element Models with Interface Reduction," *AIAA Journal*, vol. 55, pp. 1695-1706, 2017/05/01 2017.

[10] P. Wriggers, *Computational Contact Mechanics*, Second ed.: Springer-Verlag Berlin Heidelberg, 2006.